JOURNAL OF CATALYSIS 84, 288–296 (1983)

Cluster Calculations of Intermediate States in the Catalyzed Conversion of CH_3OH to CH_2O on a Cu(100) Surface

J. PAUL AND A. ROSÉN

Department of Physics, Chalmers University of Technology, S-412 96 Göteborg, Sweden

Received September 20, 1982; revised April 6, 1983

The Hartree–Fock–Slater (HFS) calculations of a CH_3OCu_5 cluster symbolizing methoxide bound to a Cu(100) surface are presented. Adsorption geometry, molecular orbitals, and symmetry properties of the CH_3O group in terms of one-electron energies, charge distributions, and partial densities of states (PDOS) are discussed. A comparison of calculated ionization energies and measured binding energies supports the occupation by methoxide of the hollow adsorption site. The electron distribution of the hydrogen atoms has been analyzed for different geometries and is shown to be a sensitive probe of the oxidation from methoxide (CH_3O)/methyl (CH_3) to formaldehyde (CH_2O)/methylene (CH_2).

INTRODUCTION

Methoxide, CH_3O, has been identified as an adsorbed intermediate on various metal surfaces in the catalytic conversion of methanol to a variety of small organic molecules. On platinum (*1*), ruthenium (*2*), and nickel (*2–5*) surfaces the dominant final products are CO and H_2 (also some H_2O, CO_2, O, CH_4, CH_2O) whereas on Cu(100) and Cu(110) surfaces only one proton is stripped off the methyl group and the molecule instantly desorbs as formaldehyde, CH_2O (*6–14*).

Many catalytic processes involve changes of symmetry of electronic ground states along a reaction path. Hence it is of fundamental interest for reaction studies to compare how surfaces of different symmetries as well as of different densities of states at the Fermi level will influence adsorption sites, molecular eigenvalues, and ionization energies. In this paper we study the perturbations from C_{3v} (CH_3O) or C_{2v} (CH_2O) symmetry for CH_xO adsorbed on a Cu(100) surface. It should be noted that when the methoxide is adsorbed on a Cu(100) surface the highest possible symmetry of the bound complex is C_s, which represents a subgroup to both product (CH_2O) and reactant (CH_3O). We discuss in the following sections how our calculated electronic properties are related to experimental data obtained by electron energy loss spectroscopy (EELS) (*6, 7*), ultraviolet photoelectron spectroscopy (UPS) (*8–10*), infrared absorption spectroscopy (IRS) (*11–13*), and flash decomposition spectroscopy (*14*).

COMPUTATIONAL SCHEME

Calculations presented in this work are based on a quantum chemical approach where adsorption is modeled by the interaction between a molecule and a small cluster of atoms representing the surface. The nonrelativistic Hamiltonian for an electron (i) is given as

$$h_i = -\tfrac{1}{2}\nabla_i^2 + V(r).$$

$V(r)$ represents the molecular potential taken as the sum of the Coulomb and exchange terms. The Coulomb potential, $V_c(r)$, describes the sum of nuclear and electronic contributions.

$$V_c(r) = -\sum_A \frac{Z_A}{|r - R_A|} + \int_V \frac{dr'\rho(r')}{|r - r'|}.$$

0021-9517/83 $3.00

$\rho(r')$ gives the electron density. In the applied model, Hartree–Fock–Slater (HFS), the exchange terms in the Hartree–Fock equations are replaced by a local potential $V_x(r)$ (*15*):

$$V_x(r) = -3\alpha\{(\tfrac{3}{8}\pi)\rho(r)\}^{1/3}.$$

α, which represents the strength of this potential, has been chosen to be equal to 0.70. The molecular wavefunctions are approximated by linear combinations of atomic orbitals (LCAO) combined as symmetry orbitals to reduce the number of nonvanishing matrix elements. Integrals are numerically evaluated in the discrete variational method (DVM) (*16*). Radial wave functions are generated as numerical atomic basis functions in the Cu $3d^{10}4s^14p^0$, O $2s^22p^4$, C $2s^22p^2$, and H $1s^12s^0$ configurations by an atomic HFS program. The molecular potential is determined in the successive iterations from Mulliken gross orbital occupation numbers (*17*) of these atomic basis functions. Self-consistency is obtained when the input and output occupation numbers are equal, the self-consistent-charge (SCC) procedure (*18*). Binding energies are evaluated separately as *transition state energies* (*15*). Partial densities of states (PDOS) are defined as a projection of molecular states on atomic orbitals according to a Mulliken charge analysis. Different PDOS can be summed, e.g., to show the CH_3O induced states of the adsorbed complex. By summing over all atomic orbitals we obtain the total DOS.

The numerical DVM procedure used in these calculations is at present not accurate enough for the calculation of total energies. We have thus emphasized our analysis on the evaluation of one-electron properties such as eigenvalues, binding energies, and atomic charges. The SCC method uses a local exchange potential which is a realistic approach for large molecules and solids when it markedly reduces the computational effort compared with a more *ab initio* Hartree–Fock calculation. Alternative approaches are semiempirical calculations such as CNDO and INDO (*19–21*). Even though an LCAO-Xα method such as SCC has proven to be more accurate, applied to small molecules (*22*), than, e.g., the "muffin-tin" approach of HFS-scattered wave theory (*23*), there are still certain approximations to be discussed. The first and most fundamental for metal surfaces is the limited number of substrate (adsorbent) atoms. It is, naturally, disadvantageous to discuss bonds to surface atoms which have artificially low coordination numbers. We would thus prefer to expand the present model to include a surrounding half-sphere of metal atoms. We are, however, limited by computational time since the low symmetry, C_1 (or C_s), of the adsorbed complex will not reduce the number of matrix elements. Improvements can secondly be achieved by extended or double basis sets on crucial atoms and by a multipolar expansion of the molecular charge density (*24*). The SCC method represents a nonparametrized procedure utilizing the Xα approximation for the exchange potential. Alternative potentials such as different α values for each atom (*25*) or a potential adapted to a free electron gas (*26*) do not markedly alter our results.

As a concluding remark we believe that our model gives a fairly accurate description of localized adsorbent-adsorbate bonds; however, care has to be taken when discussing delocalized states.

The coordinates for the free and adsorbed CH_3OH, CH_3O, and CH_2O molecules were fixed at experimental values (*27*). More recent experimental and theoretical geometries (*28–30*) deviate negligibly. These internal bond lengths are kept constant through all calculations of adsorbed complexes. The HFS one-electron energies are given as *ground state energies* in all figures but Fig. 2.

RESULTS AND DISCUSSION

Adsorption Geometry

There are strong experimental indications that methoxide is bound in a hollow

position on a Cu(100) surface (*6, 7*). We use a five-atom cluster to represent this site in our calculations. The proposed geometry with the variables h, θ, and ϕ are shown in Fig. 1. The discrepancy between different experiments concerning the symmetry of the adsorbed methoxide molecule (*6, 7, 9, 11, 31, 32*) stems from the limited sensitivity of vibrational and electron spectroscopy to small deviations from, e.g., C_{3v}. Strictly speaking, one has to analyze the subgroup decomposition of different point groups to find the symmetries of adsorbed complexes. These ground state symmetries may, however, be broken by various excitations as well as trajectories, neighboring adsorbates, etc. The highest symmetry of CH_3O on Cu(100), C_s, is obtained for arbitrary θ when $\phi = 0$ or 45°.

The subscripts of atoms in our formulas indicate averaging of occupation numbers for atoms which are equal or nearly equal for a certain geometry. We analyze in the calculations deviations from an unperturbed methyl group by assigning separate potentials to the 2 + 1 hydrogen atoms when the adsorbed complex, CHH_2OCu_5, belongs to the C_s point group. Not explicitly considered in these calculations are the averaging effects of rotations round the C–O axis and the height of this rotational barrier (*33*).

Since at present we do not calculate total energies we use the ionization energies of adsorbed molecules to determine the height above the metal surface. This procedure has successfully been applied to the CO/Cu(111) adsorption system (*34*). For CH_3O bound to a Cu(100) surface such a comparison is shown in Fig. 2 in which ionization energies for CH_3O are calculated at varying h distances ($\theta = \phi = 0$). The peaks of the experimental photoemission spectra for s and p polarized light converge at $h = 2.0$ a.u. The symmetries of the unperturbed CH_3O molecular orbitals agree with UPS data since s polarized light does not excite a_1 orbitals (*9*). This excellent agreement is probably fortuitous and slight shifts are likely to occur when going beyond the SCC procedure. The measured peaks are similar to those of CH_3O bound to a Cu(110) surface where a fourth peak is found 15.5 eV below the Fermi level (*8*). That peak is accounted for by the $4a_1$ orbital. The similari-

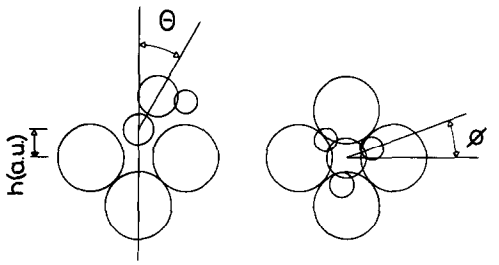

FIG. 1. The geometry of the cluster symbolizing methoxide, CH_3O, adsorbed in a hollow site on a Cu(100) surface. h represents the height of the oxygen atom above the surface, θ the tilting angle, and ϕ the rotation of the methyl group.

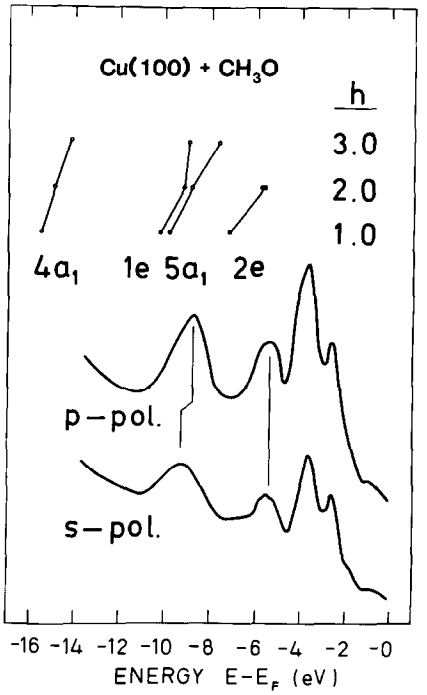

FIG. 2. Calculated HFS *ionization energies* for three different values of h (Fig. 1) compared with photoemission data (*9*) for s and p polarized light (21.2 eV). $4a_1$, etc., are the molecular orbitals of a free CH_3O radical. We have no data for the "2*e*" orbital when h equals 3.0 a.u. since it cannot be separated from the copper 3*d* states at this distance.

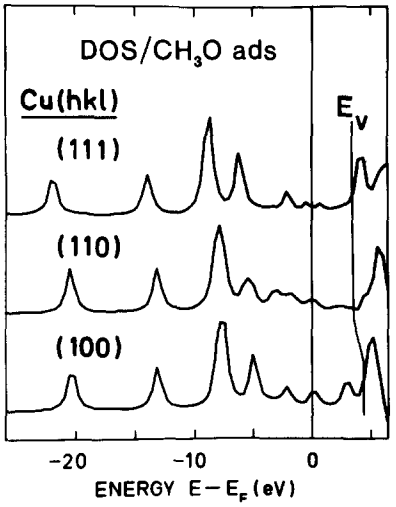

FIG. 3. Density of methoxide states for the hollow position of three different copper substrates represented by small clusters (3–5 atoms). h is 2.0 a.u. for the (100) surface and the Cu–O distance is kept constant for all surfaces.

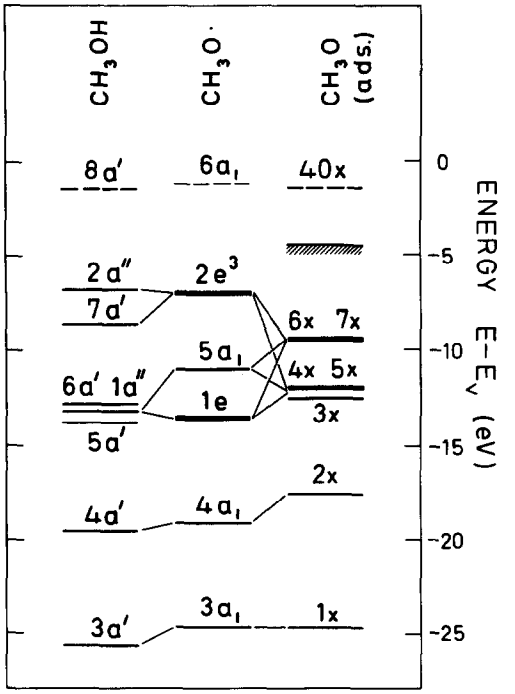

FIG. 4. Molecular eigenvalues of free methanol and methoxide compared to the electronic states of adsorbed CH_3O (h = 2.0 a.u.). Thin lines indicate how orbitals mix. Dashed states are unoccupied. The Fermi level is shown for adsorbed CH_3O.

ties between the (100) and (110) surfaces are also seen in Fig. 3 where we compare the CH_3O density of states (DOS) for three different surfaces represented by small clusters (3–5 atoms) centered around a hollow adsorption site.

The Chemisorption Bond

To understand some of the properties of adsorbed methoxide we have visualized in Fig. 4 the eigenvalues and the mixing of orbitals for free CH_3OH, CH_3O, and CH_3O adsorbed at h = 2.0 a.u. These orbitals should be related to the density of methoxide states for different h values (Fig. 5) as well as the net charges shown in Fig. 6. The latter which are obtained by an analysis of the Mulliken gross occupation numbers of atomic orbitals contain information not only about chemical bonds but also about polarization effects (*35*). Schematic drawings of methanol orbitals are given in Ref. (*36*). The nonbonding O 2p orbitals of methanol (2a'' and 7a') are degenerate for the methoxide radical (2e^3). In Fig. 5 these 2e orbitals appear as a peak at the Fermi level ($h = \infty$). These reactive states of the oxygen atom couple strongly to the adsorbent at large distances (h = 3.0 a.u.). However, at this distance the CH bonds (1e) are unaffected. This is readily seen in Fig. 6 since the CH_3 net charge is constant for CH_3OH (a), CH_3O (b), and CH_3O adsorbed at h = 3.0 a.u. (c) whereas the oxygen net charge is drastically changed. However, for h less than or equal to 2.0 a.u. (d–f) there is a marked influence on the methyl group. This results in a split of the main C–H peak, 1e to 3–7 x, for $h \leq$ 2.0 a.u. What in Fig. 5 appears as a rigid shift of orbitals between $h = \infty$ and h = 2.0 a.u. is thus a result of mixed orbitals (Fig. 4).

This mixing process is deepened and involves the 2x orbital for an artificial geometry where h equals 0.0 a.u. Note, however, that the in-plane adsorption of the oxygen

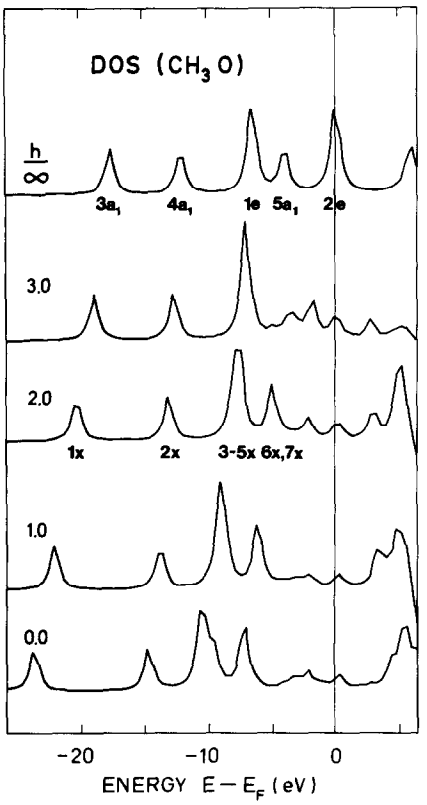

FIG. 5. Density of CH_3O states for different h values above a hollow position on a Cu(100) surface. The CO axis is normal to the surface, i.e., $\theta = \phi = 0$.

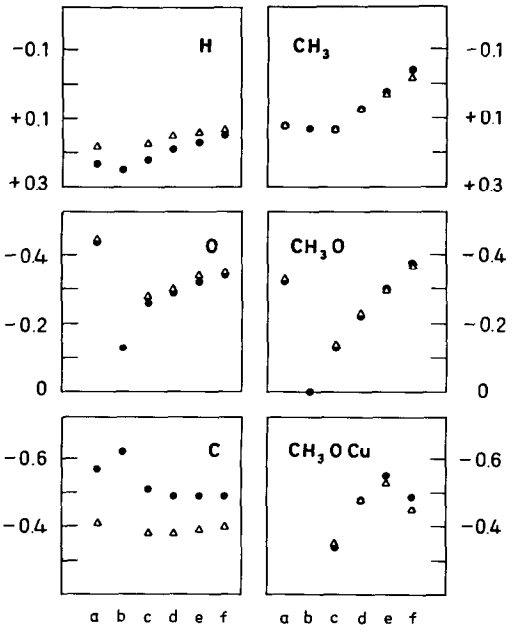

FIG. 6. Net charge per item as given by a Mulliken analysis. The H values are given as an average value over the 3 hydrogen atoms in the methyl group. (a) Free CH_3OH, (b) $CH_3O\cdot$, i.e., $h = \infty$, (c) to (f) CH_3O adsorbed at h 3.0, 2.0, 1.0, and 0.0 a.u. above Cu_5, respectively. Dots show data for the CH distance of methanol whereas triangles indicate a 10% increase of this distance. The charge of the copper atom in the second layer (Fig. 1) is included in the CH_3OCu diagram.

atom corresponds to the Cu–O separation for copper oxide, 3.3 a.u. The lowest unoccupied molecular orbital (LUMO) of methanol, $8a'$, which is characterized as an antibonding σ_{CO} orbital (*36*), is constant in energy (Fig. 4) even though it is mixed with antibonding CH orbitals. Further details about the perturbed methyl group, charge distributions, and unoccupied states will be discussed below.

Methyl to Methylene

Having established a probable geometry of the adsorbed CH_3O molecule we can proceed to analyze the electron distribution in some detail. Since the main feature of the catalyzed reaction of adsorbed CH_3O to CH_2O is the conversion of the methyl group to a methylene group we will analyze the hydrogen electron distribution. Figure 7 shows the PDOS for the hydrogen atoms of the methyl group (underlined). Thus we discern only one difference on the methyl group when the hydroxyl hydrogen atom is removed. The $7a'$ and $2a''$ are no longer separated which is reasonable since the nonbonding O $2p$ orbitals are degenerate in a C_{3v} configuration. These orbitals at the Fermi level form the reactive part of the methoxide molecule. Further down in Fig. 7 we see the PDOS/H of adsorbed CH_3O when separated as H_1 (dashed) and H_2 (full line) for $h = 2.0$ a.u. We note that the occupied states are similar and thus the C_{3v} symmetry of the methyl group is preserved. However, the main peak ($5a'$, $1a''$) of the CH_3OH molecule has been split.

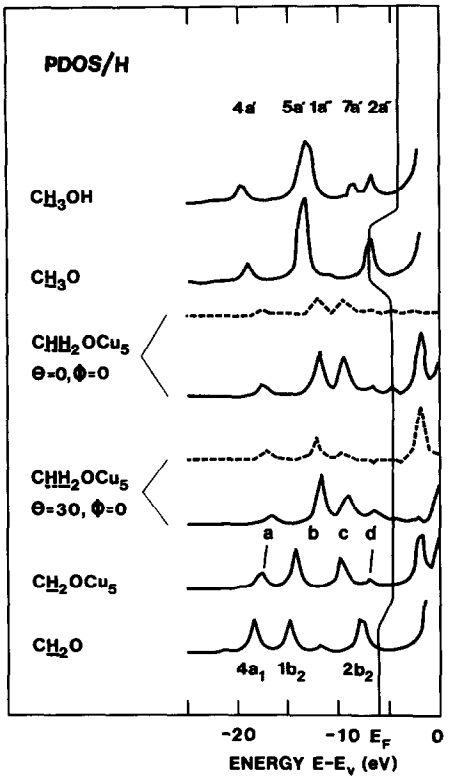

FIG. 7. Partial densities of states for the underlined hydrogen atoms. From top to bottom we show the data for methanol, free methoxide, methoxide bound at h = 2.0 a.u. with the CO axis normal to the surface or tilted and finally adsorbed, and free formaldehyde. Relevant molecular orbitals of free CH_3OH and CH_2O are denoted above each peak. The PDOS for the adsorbed methoxide are separated as H_1 (dashed) and H_2 (full lines) to include deviations from C_{3v} symmetry. (a) to (d) Orbitals discussed in the text.

When the molecule is tilted (30°) (*11, 14*) we note a separation of the orbital energies of H_2 and H_1, the latter noding toward the surface (Fig. 1). A similar effect is also seen for a tilted molecule when ϕ equals 45° (not shown). If we analyze the electron distribution of formaldehyde adsorbed in a similar tilted position CH_2OCu_5, we find four peaks (a–d) as well for the two equal hydrogen atoms of the tilted methoxide. These four orbitals have similar compositions and support the stripping mechanism proposed by Wachs and Madix for CH_3O on Cu(110) (*14*). However, these orbitals a–d are slightly shifted in energy from tilted CH_3O to CH_2O. Without the support of total energy calculations we do not adjust bond lengths of adsorbates when bound to metal clusters. The CH_2OCu_5 calculation is performed with the CH_2O molecule tilted 30° and the C atom fixed at the position of the tilted CH_3O group. The free CH_2O molecule is shown below the adsorbed species. The difference between the adsorbed and free CH_2O molecule represents the desorption mechanism which is beyond the scope of this work.

Vibrational Excitations

It has recently been proposed that an antibonding CH resonance level at the Fermi level is responsible for the broadened absorption lines (*12*) observed for the CH stretch vibrations of the adsorbed methoxide (*11*). As previously mentioned (Fig. 5) we do, however, only find minor shifts of states around the Fermi level for adsorbed methoxide. This is clearly seen for the methyl group in Fig. 7. In Fig. 6 we have analyzed the net charges of different geometries with either normal C–H separation (dots) or with an artificial 10% increase of these bond lengths (triangles). (a) Represents CH_3OH, (b) $CH_3O\cdot$, i.e., $h = \infty$, (c) CH_3OCu_5 with h = 3.0 a.u. and $\theta = \phi = 0°$, (d) h = 2.0 a.u., (e) h = 1.0 a.u., and (f) h = 0.0 a.u. We conclude from this analysis that hardly any charge moves to and fro from the methyl group for any reasonable upright geometry when CH vibrations are excited.

This is plausible even if we believe a jellium to give a more appropriate description of the charge tail above the surface (Fig. 8). In the jellium model a valence electron gas resides within a potential consisting of a uniform rigid background of positive charge plus a term for the electron–electron interaction (*37*). This model suppresses in its original form the discrete atomic character of condensed matter. Hence it is most appropriate for metals such as the alkali

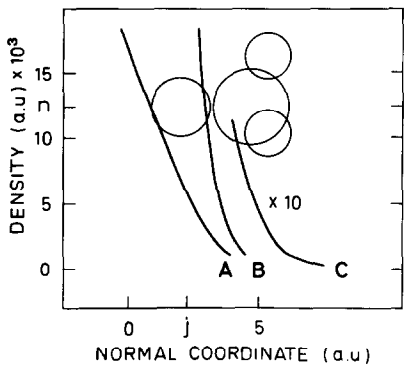

FIG. 8. Adsorbed methoxide compared to the unperturbed electron density above a Cu(100) surface. (A) Hollow and (B) top site stem from a slab calculation (*39*) whereas (C) is a Cu jellium tail (*37*) adjusted to the (A) curve. (n) is the bulk electron density and (j) is the jellium edge.

metals. Recent extensions such as the effective-medium theory (*38*) broaden its applicability to include transition metals.

An unperturbed copper jellium (*37*) gives a dilute electron gas of 4.0×10^{-4} a.u. at the suggested position of the methyl group. We show in Fig. 8 the electron density above a hollow (A) and a top (B) position as evaluated by a slab calculation (*39*). The copper jellium edge (j) of a bulk electron density (n) is adjusted to the (A) curve.

Our cluster approach to chemisorption has the limitations of a limited basis set and a small number of substrate (adsorbent) atoms. From a previous successful study of the $2\pi^*$ resonance of CO on Cu(111) (*34*) we believe that our discrete set of electronic states gives a fair description of localized adsorbent–adsorbate bonds. Molecular orbitals calculated in this approach must, however, either be broadened artificially or be given appropriate asymptotic boundary conditions (*40*) to give a continuous density of states at the Fermi level. This is essential for explicit calculations of vibrational lifetimes for molecules adsorbed on metal surfaces (*41*). We will not discuss alternative dissipation mechanisms, i.e., explanations of the broad CH absorption lines (*42*).

Reaction Path

The first step in the catalyzed conversion of methanol to formaldehyde on a Cu(100) or (110) surface is the transfer of a hydrogen atom from the hydroxyl group to the copper substrate (*6, 8, 13, 14*). This step is very much enhanced by the presence of preadsorbed atomic oxygen (*8, 14*). This proton transfer leaves an adsorbed methoxide in a hollow position on a (100) surface (Fig. 2 and Refs. (*6, 7*)). We have not fully analyzed the (110) surface but predict, from the similarities of UPS data (*8–10*) and our calculated ground state energies (Fig. 3), the hollow position to be occupied also on this surface. A 30° tilt of the CH_3O group on Cu(100), which shortens the Cu–H distance from 5.6 to 3.9 a.u. (cf. CuH 2.8 a.u.), will break the C_{3v} symmetry and provide for an elementary reaction to yield CH_2O (*14*). For free methoxide radicals an alternative reaction path which involves a unimolecular isomerization of a proton from the methyl group to the oxygen atom has recently been proposed (*29, 43–46*). Such an isomerization is favored by the unpaired electron on the oxygen atom ($2e^3$ in Fig. 5). It is, however, unlikely to occur when the localized spin density becomes delocalized to the copper substrate as a result of the chemisorption bond. In a spin-unrestricted calculation of free $CH_3O\cdot$ vs CH_3O adsorbed on a Cu(111) surface (modeled by 3 or 4 Cu atoms) the net spin of the O $2p$ orbital is reduced from 0.98 to less than 0.08 electrons. This becomes further enlightened when the spin-restricted net charges (Fig. 6) of CH_3O in CH_3OH (a), $CH_3O\cdot$ (b), and CH_3OCu_5 for $h = 2.0$ a.u. (d) are compared; the reactive character of the oxygen atom of the methoxide radical is annihilated by the copper substrate.

Finally, we would like to mention a complementary model to explain the stability of the methyl–methylene group on different metal surfaces. The step following the stripping of one proton from the methyl group may be seen as an electron transfer from

the adsorbent to the C=O bond. This picture does not explicitly take into account the formation of chemisorption bonds but the process should be sensitive to the potential of the substrate (adsorbent), i.e., the work function. Such a redox description is well modeled by a jellium and should be considered when discussing the effects of different adsorbates that shift the work function, e.g., surplus or nonstoichiometric amounts of preadsorbed oxygen (*47*).

CONCLUSIONS

We compare calculated HFS ionization energies with measured binding energies for methoxide (CH_3O) on a Cu(100) surface and conclude that CH_3O occupies a hollow site with the oxygen atom toward the surface 2.0 a.u. above the first metal plane. From our computed geometry we discuss the importance of broken symmetries for the conversion of methyl (CH_3) to methylene (CH_2). A crucial experiment would be to compare the rate of formation of formaldehyde from adsorbed methoxide on the (100), (110), and (111) surfaces of copper; the C_{3v} symmetry of CH_3O can be preserved only on the (111) surface.

ACKNOWLEDGMENTS

We appreciate valuable comments by L. Melander, R. Ryberg, and L. Walldén.

REFERENCES

1. Sexton, B. A., *Surf. Sci.* **102,** 271 (1981).
2. Yates, J. T., Goodman, D. W., and Madey, T. E., "Proceedings, 7th International Vac. Congress and 3rd International Conference Solid Surfaces," 1133. Vienna, 1977.
3. Rubloff, G. W., and Demuth, J. E., *J. Vac. Sci. Technol.* **14,** 419 (1977).
4. Erskine, J. L., and Bradshaw, A. M., *Chem. Phys. Lett.* **72,** 260 (1980).
5. Demuth, J. E., and Ibach, H., *Chem. Phys. Lett.* **60,** 395 (1979).
6. Sexton, B. A., *Surf. Sci.* **88,** 299 (1979).
7. Andersson, S., and Persson, M., *Phys. Rev. B* **24,** 3659 (1981).
8. Bowker, M., and Madix, R. J., *Surf. Sci.* **95,** 190 (1980).
9. Hofman, P., Mariani, C., Horn, K., and Bradshaw, A. M., Proc. ECOSS 3, 541, Cannes, 1980.
10. Carlson, T. A., Agron, P. A., Thomas, T. M., and Grimm, F. A., *J. Electr. Spec. Rel. Phenom.* **23,** 13 (1981).
11. Ryberg, R., *Chem. Phys. Lett.* **83,** 423 (1981).
12. Persson, B. N. J., and Ryberg, R., *Phys. Rev. Lett.* **48,** 549 (1982).
13. Ryberg, R., *Phys. Rev. Lett.* **49,** 1579 (1982).
14. Wachs, I. E., and Madix, R. J., *J. Catal.* **53,** 208 (1978).
15. Slater, J. C., "The Self-Consistent Field for Molecules and Solids." McGraw–Hill, New York, 1974.
16. Ellis, D. E., and Painter, G. S., *Phys. Rev. B* **2,** 2887 (1970).
17. Mulliken, R. S., *J. Chem. Phys.* **23,** 1833, 1841, 2338, 2343 (1955).
18. Rosén, A., Ellis, D. E., Adachi, H., and Averill, F. W., *J. Chem. Phys.* **65,** 3629 (1976).
19. Pople, J. A., and Beveridge, D. L., "Approximate Molecular Orbital Theory." McGraw–Hill, New York, 1970.
20. Freund, H-J., and Hohlneicher, G., *Theor. Chim. Acta (Berlin)* **51,** 145 (1979).
21. Bacon, A. D., and Zerner, M. C., *Theor. Chim. Acta (Berlin)* **53,** 21 (1979).
22. De Alti, G., Decleva, P., and Lisini, A., *Chem. Phys.* **66,** 425 (1982).
23. Johnson, K. H., *Adv. Quant. Chem.* **7,** 143 (1973).
24. Delley, B., and Ellis, D. E., *J. Chem. Phys.* **76,** 1949 (1982).
25. Schwarz, K., *Phys. Rev. B* **5,** 2466 (1972).
26. Hedin, L., and Lundqvist, B. I., *J. Phys. C* **4,** 2064 (1971).
27. "Handbook of Chemistry and Physics," 54th ed., Chem. Rubber Co., Cleveland, 1973–74.
28. Adams, G. F., Bent, G. D., Bartlett, R. J., and Purvis, G. D., *J. Chem. Phys.* **75,** 834 (1981).
29. Adams, G. F., Bent, G. D., Purvis, G. D., and Bartlett, R. J., *Chem. Phys. Lett.* **81,** 461 (1981).
30. Yarkony, D. R., Schaefer, H. F., and Rothenberg, S., *J. Amer. Chem. Soc.* **96,** 656 (1974).
31. Bradshaw, A. M., *Z. Phys. Chem. Neue Folge* **112,** 33 (1978).
32. Ibach, H., Hopster, H., and Sexton, B. A., *Appl. Surf. Sci.* **1,** 1 (1977).
33. Fink, W. H., and Allen, L. C., *J. Chem. Phys.* **46,** 2261 (1967).
34. Paul, J., and Rosén, A., *Phys. Rev. B* **26,** 4073 (1982).
35. Paul, J., and Rosén, A., Proc. 4th ICQC (Uppsala, 1982); *Int. J. Quantum Chem.* **23,** 1237 (1983).
36. Jørgensen, W. L., and Salem, L., "The Organic Chemist's Book of Orbitals." Academic Press, New York, 1973.
37. Lang, N. D., and Kohn, W., *Phys. Rev. B* **1,** 4555 (1970).

38. Nørskov, J. K., *Phys. Rev. B* **26,** 2875 (1982).
39. Gay, J. G., Smith, J. R., and Arlinghaus, F. J., *Phys. Rev. Lett.* **38,** 561 (1977).
40. Lindgren, B., and Ellis, D. E., *Phys. Rev. B* **26,** 636 (1982).
41. Persson, B. N. J., and Persson, M., *Solid State Commun.* **36,** 175 (1980).
42. Persson, M., and Hellsing, B., *Phys. Rev. Lett.* **49,** 662 (1982).
43. Radford, H. E., *Chem. Phys. Lett.* **71,** 195 (1980).
44. Batt, L., Burrows, J. P., and Robinson, G. N., *Chem. Phys. Lett.* **78,** 467 (1981).
45. Adams, G. F., Bartlett, R. J., and Purvis, G. D., *Chem. Phys. Lett.* **87,** 311 (1982).
46. Saebø, S., Radom L., and Schaefer, H. F., *J. Chem. Phys.* **78,** 845 (1983).
47. Spitzer, A., and Lüth, H., *Surf. Sci.* **118,** 121, 136 (1982).